NASA Technical Memorandum 101376

Simulation of 3-D Viscous Flow Within a Multi-Stage Turbine

John J. Adamczyk
National Aeronautics and Space Administration
Lewis Research Center
Cleveland, Ohio

Mark L. Celestina and Tim A. Beach
Sverdrup Technology, Inc.
NASA Lewis Research Center Group
Cleveland, Ohio

and

Mark Barnett
United Technologies Research Center
Hartford, Connecticut

Prepared for the
34th International Gas Turbine and Aeroengine Congress and Exposition
sponsored by the American Society of Mechanical Engineers
Toronto, Canada, June 4–8, 1989

NASA

SIMULATION OF THREE-DIMENSIONAL VISCOUS FLOW WITHIN A MULTISTAGE TURBINE

John J. Adamczyk
National Aeronautics and Space Administration
Lewis Research Center
Cleveland, Ohio

Mark L. Celestina and Tim A. Beach
Sverdrup Technologies, Inc.
NASA Lewis Research Center Group
Cleveland, Ohio

Mark Barnett
United Technologies Research Center
Hartford, Connecticut

E-4430

ABSTRACT

This work outlines a procedure for simulating the flow field within multistage turbomachinery which includes the effects of unsteadiness, compressibility, and viscosity. The associated modeling equations are the average passage equation system which governs the time-averaged flow field within a typical passage of a blade row embedded within a multistage configuration. The results from a simulation of a low aspect ratio stage and one-half turbine will be presented and compared with experimental measurements. It will be shown that the secondary flow field generated by the rotor causes the aerodynamic performance of the downstream vane to be significantly different from that of an isolated blade row.

INTRODUCTION

A goal of computational fluid dynamics for turbomachinery is the prediction of performance parameters and the flow processes which set their values. Achieving this goal for multistage devices is made difficult by the wide range of length and time scales in the associated flow fields. Currently the procedure used in design and off design analysis is based on a quasi-three-dimensional flow model whose origins can be traced back to the late forties and early fifties, e.g., (Wu, 1952; Smith, 1966). This model requires calculations to be executed on two orthogonal surfaces within a blade row passage of a multistage configuration. One of these surfaces is an axisymmetric surface of revolution whose intersection with a blade row defines a cascade. The flow field relative to this cascade is assumed to be steady in time. In practice, a finite number of such surfaces are chosen to define a series of cascade flows from hub to shroud. The other surface represents a meridional through-flow surface. The flow associated with this surface is an axisymmetric representation of the flow field within the machine. This flow field is also assumed to be steady. The flow fields on both surfaces are coupled and are solved iteratively. The effects of unsteadiness, turbulence, and endwall secondary flows are introduced through empirical correlations.

Although proven to be very useful, this flow model has its limitations. Among these is off-design performance analysis, and the ability to analyze unconventional machinery where extrapolation of the underlying empirical database is required. Other problems arise whenever there are large local variations in the radial velocity component within a blade passage. Such variations can be brought about by in-passage shock waves, separated boundary layers, and endwall secondary flows. It is generally agreed upon that a way of overcoming these shortcomings is the development of a true three-dimensional flow model.

Two three-dimensional flow models have been proposed for the simulation and analysis of multiple blade row flows. The first (Denton, 1979; Adamczyk 1984; Ni, 1987) referred to as the average passage flow model in Adamczyk (1986) simulates the time-averaged flow field within a typical passage of the blade row. The second simulates the unsteady deterministic flow field within the machine. Although a number of unsteady simulations of single stage turbine configurations and counterrotating propellers have been reported (Rai, 1987; Whitfield et al., 1987), executing an unsteady simulation of a multistage configuration of practical interest is far beyond the capabilities of todays advanced supercomputers. Furthermore, it is by no means obvious that performance prediction requires such a high degree of flow resolution. However, because unsteady simulations of an idealized configuration may prove to be a useful means of investigating the closure issue associated with time-averaged flow models, this activity should be pursued. In this work it will be shown that the simulation of the time-averaged flow field within multistage machinery is within the capabilities of todays advanced computers and that the average passage flow model gives more insight into the flow phenomena that control the performance of multistage machinery than today's quasi three-dimensional flow models.

The objective of this paper is to outline a procedure for simulating the time averaged flow field within a typical passage of a blade row within a multistage machine. This model includes the effects of viscosity and compressibility, and the influence of neighboring blade rows. The mathematical formulation upon which

this model is based has been outlined in Adamczyk (1984). The algorithm used to solve the inviscid form of the governing equations is reported in Celestina, (1986); Adamczyk et al. (1986). The current work outlines a numerical solution procedure for the viscous form of these equations and an acceleration technique to enhance convergence. In addition, a comparison will be made between experimental data recorded during tests of a one and one-half stage, large scale, low speed, axial flow research turbine and simulation prediction. The underlying unsteady flow physics which appears to control the performance of the second vane of this machine will also be discussed.

GOVERNING EQUATION

A complete derivation of the three-dimensional average-passage equation system is presented in Adamczyk (1984). These equations were derived by filtering the Navier Stokes equation in both space and time to remove all information except that associated with the time average flow field within a typical passage of a blade row of a multi-stage configuration. With respect to this blade row, the integral form of these equations can be written

$$\int \frac{\partial}{\partial t}(\lambda q)d\forall + L(\lambda q) = \int \lambda S \, d\forall + \int \lambda k \, d\forall + L_v(\lambda q) \quad (1)$$

The vector q contains variables density, axial and radial momenta, angular momenta, and total internal energy. λ is the neighboring blade row blockage factor and ranges between zero and unity, unity being the value associated with zero blade thickness. This parameter explicitly introduces the effect of the neighboring blade row blade thickness. The operator $L(\lambda q)$ balances the mass, axial and radial momenta, angular momentum, and energy through a control volume. $\int \lambda k \, d\forall$ is a source term due to the cylindrical coordinate system and $\int \lambda S d\forall$ contains the body forces, energy sources, momenta, and energy temporal and spatial mixing correlations associated with the neighboring blade rows. A procedure for estimating S has been outlined in Adamczyk et al. (1986) and is extended here to include the effects of viscosity. The operator $L_v(\lambda q)$ contains the viscous and heat transfer terms. The vector q and the operators L and L_v are defined as

$$q = [\rho, \rho v_z, \rho v_r, r\rho v_\theta, \rho e_o]^T \quad (2)$$

$$L = \int_{dA} [\lambda \bar{F} \, dA_z + \lambda \bar{G} \, dA_r + \lambda \bar{H} \, dA_\theta] \quad (3)$$

and

$$L_v = \int_{dA} [\lambda \bar{F}_v \, dA_z + \lambda \bar{G}_v \, dA_r + \lambda \bar{H}_v \, dA_\theta] \quad (4)$$

where

$$\bar{F} = [\rho v_z, \rho v_z^2 + P, \rho v_z v_r, r\rho v_z v_\theta, \rho H v_z]^T \quad (5)$$

$$\bar{G} = [\rho v_r, \rho v_2 v_r, \rho v_r^2 + P, r\rho v_r v_\theta, \rho H v_r]^T \quad (6)$$

$$\bar{H} = [\nu n_\theta, \rho v_\theta v_z, \rho v_\theta v_r, r(\rho v_\theta^2 + P), \rho H v_\theta]^T \quad (7)$$

$$\bar{F}_r = [0, \tau_{rr}, \tau_{zr}, \tau_{z\theta}, q_z]^T \quad (8)$$

$$\bar{G}_r = [0, \tau_{zr}, \tau_{rr}, \tau_{r\theta}, q_r]^T \quad (9)$$

$$\bar{H}_v = [0, \tau_{\theta z}, \tau_{\theta r}, \tau_{\theta\theta}, q_\theta]^T \quad (10)$$

$$\bar{\tau}_{zz} = 2\mu \frac{\partial v_z}{\partial z} + \lambda_v \vec{\nabla} \cdot \vec{V} \quad (11)$$

$$\tau_{zr} = \tau_{r2} = \mu \left(\frac{\partial v_r}{\partial z} \right) + \left(\frac{\partial v_z}{\partial r} \right) \quad (12)$$

$$\tau_{z\theta} = \tau_{\theta z} = \mu \left(\frac{1}{r} \frac{\partial v_r}{\partial \theta} \right) + \left(\frac{\partial v_\theta}{\partial z} \right) \quad (13)$$

$$\tau_{rr} = 2\mu \left(\frac{\partial v_r}{\partial r} \right) + \lambda_v \vec{\nabla} \cdot \vec{V} \quad (14)$$

$$\tau_{r\theta} = \tau_{\theta r} = \mu \left(\frac{1}{r} \frac{\partial v_r}{\partial z} + \frac{\partial v_\theta}{\partial r} - \frac{v_o}{r} \right) \quad (15)$$

$$\tau_{\theta\theta} = 2\mu \left(\frac{1}{r} \frac{\partial v_\theta}{\partial \theta} + \frac{v_r}{r} \right) + \lambda_v \vec{\nabla} \cdot \vec{V} \quad (16)$$

$$q_z = \nu_z \tau_{zz} + \nu_r \tau_{zr} + \nu_\theta \tau_{z\theta} \, k \frac{\partial T}{\partial z} \quad (17)$$

$$q_r = \nu_z \tau_{rz} + \nu_r \tau_{rr} + \nu_\theta \tau_{r\theta} + k \frac{\partial T}{\partial r} \quad (18)$$

$$q_o = \nu_z \tau_{\theta z} + \nu_\theta \tau_{\theta r} + \nu_\theta \tau_{\theta\theta} + k \frac{1}{r} \frac{\partial T}{\partial \theta} \quad (19)$$

$$k = \left[0, 0, \frac{\rho v_\theta^2 + P}{r} - \tau_{\theta\theta}, 0, 0 \right]^T \quad (20)$$

In the above equations ρ represents the density, $\vec{v}$ the absolute velocity vector, p the pressure, and T the temperature. The differential $d\forall$ is the volume of the control volume and dA_z, dA_r, dA_θ are the differential areas of its sides. From the equation of state, the total internal energy is related to pressure through the equation

$$e_o = \frac{P}{\rho(\gamma - 1)} + \frac{1}{2} |\vec{v}|^2 \quad (21)$$

and the total enthalpy, H, is related to p and e_o by

$$H = e_o + \frac{p}{\rho} \quad (22)$$

Sutherland's law is used to determine the molecular viscosity coefficient, and Stokes' hypothesis gives $\lambda_v = -2/3 \, \mu_\ell$. Turbulence is accounted for by adding a turbulent viscosity μ_t to the molecular viscosity μ_ℓ

$$\mu = \mu_\ell + \mu_t \tag{23}$$

In a similar manner, the molecular thermal conductivity k is replaced by

$$k = C_p\left[\frac{\mu}{P_r}\bigg|_\ell + \frac{\mu}{P_r}\bigg|_t\right] \tag{24}$$

where C_p is the specific heat at constant pressure and $P_r|_\ell + P_r|_t$ is the laminar and turbulent Prandtl number respectively. The two-layer algebraic model of Baldwin and Lomax (1978) is used to model μ_t.

All lengths in the above equations are nondimisionalized by a reference length normally taken as the largest blade row diameter. The velocity components are nondimsionalized by a reference speed of sound, $a_{ref}/\ \gamma$ where γ is the ratio of specific heats. Pressure and density are nondimensionalized by their respective reference values.

For rotating flows, the absolute (fixed) reference frame is transformed to the relative (rotating) frame by the transformation

$$\theta_{ABSOLUTE} = \theta_{RELATIVE} + \Omega t \tag{25}$$

where Ω is the rotational wheel speed. Introducing Eq. (24) into Eq. (1) transforms L and L_v to

$$L = \int_{dA}\left(\lambda\bar{F}\ dA_z + \lambda\bar{G}_v dA_r + \lambda(\bar{H} - r\Omega q)dA_\theta\right) \tag{26}$$

and

$$L_v = \int_{dA}\left(\lambda\bar{F}_v\ dA_z + \lambda\bar{G}_v dA_r + \lambda(\bar{H}_v - r\Omega q)\ dA_\theta\right) \tag{27}$$

Discretization of the inviscid portion of Eq. (1) including estimates of the surface area and volume is presented in Celestina et al. (1986). The viscous and heat transfer portion of Eq. (1) is discretized by evaluating the shear stress and the heat flux at the center of each face. The shear stresses and heat flux are estimated using central differences of the velocity and the temperature field.

ARTIFICIAL DISSIPATION

To suppress odd-even point decoupling of the solution to the discretized equations, dissipative terms are added to the equations. The operator L_v is replaced in the discretized form of Eq. (1) with $D(\lambda q)$

$$D(\lambda q) = D_I(q) + L_v(\lambda q) \tag{28}$$

where $D_I(q)$ is the added artificial dissipation operator needed to prevent decoupling of the solution within inviscid regions of the flow. The operator D_I is patterned after the model developed by Jameson et al. (1981) and is composed of three spatial operators.

$$D_I(q) = (D_z + D_r + D_\theta)q \tag{29}$$

which can be evaluated separately. The dissipation in, for example, the axial direction (and similarly for the others) is expressed as follows:

$$D_z = d_{i+1/2,j,k} - d_{i-1/2,j,k} \tag{30}$$

where

$$d_{i+1/2,j,k} = \varepsilon^{(2)}_{i+1/2,j,k}(\Delta_z q_{i+1/2,j,k}) - \varepsilon^{(4)}_{i+1/2,j,k}\left(\Delta_z^2(\Delta_z q_{i+1/2,j,k})\right) \tag{31}$$

$$\varepsilon^{(2)}_{i+1/2,j,k} = \kappa^{(2)}_i \beta_{i+1/2,j,k} \min(\nu_{i,j,k};\ \nu_{i+1,j,k};\ 0.5) \times \min\left(\frac{M_{i+1/2,j,k}}{\bar{M}},1\right) \tag{32}$$

$$\varepsilon^{(4)}_{i+1/2,j,k} = \max\left(0,\kappa^{(4)}\beta_{i+1/2j,k},\min\left(\frac{M_{i+1/2,j,k}}{\bar{M}},1\right) - \varepsilon^{(2)}_{i+1/2,j,k}\right) \tag{33}$$

and

$\kappa^{(2)}$, $\kappa^{(4)}$ are constants set at 1/8 and 1/512 respectively. The symbols Δ and Δ^2 denote the first and second difference operators, while β is the maximum eigenvalue of the Jacobian matrix formed from $\bar{F}$. The coefficient $\nu_{i,j,k}$ is defined as

$$\nu_{i,j,k} = \left|\frac{P_{i+1,j,k} - 2P_{i,j,k} + P_{i-1,j,k}}{P_{i+1,j,k} + 2P_{i,j,k} + P_{i-1,j,k}}\right| \tag{34}$$

and is used primarily to prevent oscillations near stagnation points and shocks.

Vatsa and Wedan (1988) scaled the Jameson artificial dissipation operator by a function of the local Mach number to reduce its effect within viscous regions of the flow. The present work uses the local meridional Mach number $\bar{M}$ normalized by a reference upstream meridional Mach number $\bar{M}$ to accomplish this task. To prevent this function from increasing the level of dissipation in the inviscid flow regions, the maximum value of this function is taken as unity. To reduce the level of artificial viscosity resulting from highly stretched mesh cells, we also adopted what is referred to by Vatsa and Wedan as individual eigenvalue scaling of the artificial dissipation operator.

SOLUTION PROCEDURE

The discretized form of the equations associated with the averaged passage flow model are solved using a dimensional sequencing algorithm. The motivation for the present algorithm came from observing the evolution of the error history associated with the algorithm reported in Celestina (1986). For many cases the magnitude of the error associated with the axisymmetric component of a variable was a significant fraction of the magnitude of the error associated with the variable itself. It thus seems reasonable to expect a solution algorithm which explicitly reduced the error of the axisymmetric component of the flow field would enhance the convergence of the three-dimensional field. With the body forces assumed known, (i.e., S assumed known) the present algorithm iterates between the three-dimensional flow equations and the corresponding through-flow equations to enhance the rate of convergence to the three-dimensional time asymptotic flow problem. The construction of this algorithm is as follows. First, the through-flow equations compatible with Eq. (1) are derived by summing Eq. (1), as modified according to the discussion in the preceding sections, over the tangential index k. This is accomplished by premultiplying Eq. (1) by the operator

$$\mathscr{L} = \frac{1}{k}\sum_{k=1}^{k} \tag{35}$$

where K is the number of control volumes spanning the pitch. The result may be written as

$$\frac{d}{dt}\overline{\lambda q}\,d\bar{\forall} + \bar{L}(\bar{q}) - \bar{D}(\bar{q}) = \int \overline{\lambda k}\,d\bar{\forall} + \mathscr{L}\int S\,d\forall + \left\{\mathscr{L}\int \lambda k\,dv - \int \bar{\lambda}\,\bar{k}\,d\bar{\forall} + \bar{L}(\bar{\mathscr{L}}q) - L(q) - \bar{D}(\bar{\mathscr{L}}q) + \mathscr{L}D(q)\right\} \quad (36)$$

where $d\bar{\forall}$, $\bar{\lambda}$, $\bar{q}$ are defined as (37)

$$\mathscr{L}\lambda\,d\forall = \bar{\lambda}\,d\bar{\forall} \quad (38)$$

$$\mathscr{L}\lambda\,d\forall = \overline{\lambda q}\,d\bar{\forall} \quad (39)$$

while the operators $\mathscr{L}$, $\bar{L}$ and $\bar{D}$ are

$$\mathscr{L}\,q = \frac{\lambda q\,d\forall}{\bar{\lambda}\,d\bar{\forall}} = \bar{q} \quad (40)$$

$$\bar{L}(\bar{q}) = \mathscr{L}L(\bar{q}) \quad (41)$$

$$\bar{D}(\bar{q}) = \mathscr{L}D(\bar{q}) \quad (42)$$

The terms which appear on the right hand side of Eq. (36) are treated as forcing functions and are estimated using the most recent value of the three-dimensional flow variables. Note that the expressions which appear within brackets vanish by construction in regions of the flow where $q = \bar{q}$, and upon convergence of Eq. (36) (i.e. $\partial/\partial t \int \lambda q\,d\forall = 0$) $\bar{\mathscr{L}}q = \bar{q}$. The time asymptotic solution of Eq. (36) is thus identical to the axisymmetric average of the time asymptotic solution to Eq. (1). The steady state solution of Eq. (1) can thus be obtained by cycling between a time-advancing algorithm for Eq. (1) and a similar algorithm for Eq. (36).

The discretized form of Eq. (1) is advanced in time using the four-stage Runge Kutta algorithm of Jameson et al. (1981). Local time stepping (i.e., constant C.F.L. number) and residual averaging is employed to enhance convergence. Upon completing of a fixed number of temporal relaxation cycles, the three-dimensional flow variables are used to evaluate the right hand side of Eq. (36). This equation is then advanced in time using the same integration procedure as that for the three-dimensional system. After a fixed number of time steps, the value of q is updated according to the equation

$$q = \bar{q} + (q - \mathscr{L}q) \quad (43)$$

where the q's within the brackets are those that were used to evaluate the right from hand side of Eq. (36).

The three-dimensional residual error based on the updated value of q (i.e., Eq.(43)) is generally found to be largest within the blade passage region. Prior to initiating the next three-dimensional iteration cycle, the residual is reduced by performing a fixed number of three-dimensional iteration cycles (between five and ten iterations) over a local three-dimensional flow region which extends a modest distance upstream and downstream of the blade passage leading and trailing edges. The inlet and exit boundaries of this reduced flow domain are located in a region where the sum of the bracketed terms in Eq. (36) is small. The inlet and exit boundary conditions associated with the reduced flow domain are derived using the updated variables obtained from Eq. (43). Within this region of flow the values of q obtained from relaxing the reduced flow domain equations replace those obtained from Eq. (43).

The outlined solution procedure is a multigrid algorithm of the form introduced by Brandt (1982). It was specially constructed to reduce the axisymmetric component of the error vector, which at the start of the solution procedure is often large. It also recognizes the spatial relaxation of the three-dimensional flow field to an axisymmetric field away from the blade row of interest. This recognition reduces the computational work required to obtain a solution relative to a more traditional multigrid strategy.

The solution procedure outlined above has been implemented in both a V and W cycle framework. In the V cycle strategy, one proceeds directly from the three-dimensional solver to the through-flow solver to the reduced flow solver before going back to the three-dimensional solver. In the W cycle, one preceeds from the three-dimensional solver to the through-flow solver to the reduced flow solver and then cycles between the through-flow solver and the reduced flow solver before going back to the three-dimensional flow solver. The simulation to be reported was executed using the V cycle strategy. Experience with the W cycle is limited and needs further development. However, a preliminary analysis showed the W cycle strategy to require less computational work than the V cycle to converge to a fixed tolerance level.

When the three-dimensional flow field converges to a predetermined level, the body forces and energy sources required as input to simulations of the remaining blade rows can be estimated using the procedure outlined in Ref. 9. The cycling of information between the simulated blade rows of the multiblade row machine is carried out until the tangential average of each simulated blade row flow field agrees with each other to a predetermined tolerance.

BOUNDARY CONDITIONS

All solid surfaces are modeled as rigid, nonslip, and impermeable. The surfaces are also assumed to be adiabatic. These conditions imply that the velocity relative to a solid surface is zero and that the temperature gradient normal to the surface is also zero. The pressure at a solid surface is obtained from the normal momemtum equation evaluated at the surface. At the inlet, either the mass flow or the total pressure is specified along with the total temperature and the radial and tangential velocity components. The one-dimensional Reinmann invariant C^- is extrapolated from the interior to the boundary; with the specified flow variables, it defines the incoming pressure, axial velocity component, and temperature. The shear stresses and heat flux at the inlet are also set to zero. At the exit radial equilibrium, with the pressure specified at the hub, is used to establish the radial pressure distribution. The flow quantities ρ, ρv_z, ρv_r, ρv_θ are extrapolated from the interior.

GRID GENERATION

As discussed in Celestina et al. (1986), the averaged passage equation system requires that a mesh be specified for each blade row of a multistage machine. In addition, the meshes must have a common meridional

mesh in order to eliminate the need for interpolating the body forces and correlations from grid to grid. To capture shear layers and stagnation points properly a fine mesh spacing is required in a direction normal to solid surfaces and in the blade leading and trailing edge regions. A mesh generator which is capable of generating these features is discussed in detail in Mulac (1986).

RESULTS AND DISCUSSION

The simulation executed was the Low-Speed Rotating Rig. at United Technologies Research Center. The Low-Speed Rotating Rig (LSRR) is a stage and a half turbine consisting of an inlet guide vane, a rotor, and a stator. The inlet guide vane contains 22 blades and the rotor and stator both contain 28 blades. The flow coefficient, ϕ, is 0.78 and the spacing between blades, B_x, is 0.5. The LSRR grid contains 228 axial, 25 radial, and 41 circumferential points. Each blade row contains 40 axial points distributed along the chord with 26 axial points between each blade row, the inlet and exit.

The results to be presented required eleven hours of Cray 2 C.P.U. time. They represent but a small fraction of the information obtained from the simulation. They are intended to illustrate the degree to which one can quantitatively predict performance parameters which are of interest to designers, and to reveal qualitative information identifying flow phenomena which may have an impact on performance. These results also reflect the current state of model development. The first series of results shows the predicted pressure distribution on the surface of each blade row of the turbine as a function of axial chord length and percent of span height. The span locations measured from the hub are 1.3, 12.5, 50, 87.5 and 98.7 percent, respectively. The experimental measurements taken at these locations are also shown. Experimental data was also available for 25 and 75 percent of span but was not utilized since it provided little additional information relative to the current discussion. The results for the first vane are shown in Fig. 1. The predicted loading level is seen to be in good agreement with the measurements of Dring (1988). The predicted pressure surface pressure distribution is in excellent agreement with the experimental results. For the suction surface, the agreement between measurement and simulation is good for the region forward of the minimum pressure peak. Aft of the peak, the agreement between experiment and simulation deteriorates. This deterioration is believed to be related to viscous effects (i.e., turbulence and transition modeling) whose modeling could be improved. Some exploratory calculations suggest that the boundary layer aft of the suction surface minimum pressure is growing too rapidly and, as a result of the radial pressure gradient, is being transported towards the hub to an extent greater than that suggested by a flow visualization studies. Improvements in the agreement between simulation and experiment have been obtained by incorporating a simple transition model in which the flow remains laminar forward of the minimum pressure peak and Baldwin Lomax turbulence model as implemented by Dawes (1986). The current simulation assumes the flow to be fully turbulent from the leading edge of each blade. Work on this problem is continuing. The next figure shows the predicted and measured pressure distribution for the rotor. The predicted loading levels appear to be in good agreement with measurements, with the exception of the hub and tip region. The present simulation does not include a clearance region, which should account for some of the discrepancy in the tip region. The pressure distribution along the pressure surface is once more in excellent agreement with the measurements. At the midspan and at 25 and 75 percent (not shown) of span the predicted pressure distribution along the suction surface is in good agreement with the data. At 1.3 percent and 12.5 percent of span, the suction surface pressure coefficient is lower than that measured. As a result the loading is lower over the forward portion of the rotor than what has been measured. Although the cause of this discrepancy is unknown at the present time, one could speculate that it may be due to an overestimate of the magnitude and extent of the low momentum fluid exiting the first vane.

The pressure distribution for the last vane is shown in Fig. 3. Once again the loading level is well predicted with the exception of location that is 1.3 percent of span. The underpredicted suction surface pressure coefficient at 1.3 percent of span. The underpredicted suction surface pressure coefficient at 1.3 and 12.5 percent of span suggests that the flow incidence to these sections is underestimated. There also appears to be a shift of the predicted pressure distribution relative to the measured distribution. This shift is believed to be caused by an over estimate of the loss generated by the first two blade rows. With the exception of this discrepancy, the pressure distribution on the pressure surface is in good agreement with measurements. Similarly, the predicted suction surface distribution at midspan agrees well with the experimental distribution. The next figure shows the predicted relative total pressure coefficient forward and aft of the rotor as a function of span. The measured distribution reported in Sharma et al. (1988) is also shown. The magnitude of the predicted coefficient for the inlet flow is higher than measured; however, the shape of the curve is consistent with the data. The magnitude of the predicted exit flow coefficient is also higher than measured. The influence of the secondary vortices generated within the rotor passage on the exit flow coefficient is more evident in the experimental data than in the simulation result. The data in Sharma et al. (1988) suggests that the secondary vortices exit the rotor at approximately 30 and 70 percent of span. The local minimums in the measured exit flow distribution at 25 and 85 percent of span are a consequence of the velocity field induced by these vortices. The location of the tip vortex as suggested by the experimental data is significantly inboard of the location 90 percent span suggested by the simulation. The difference is believed to be due to the tip leakage flow which was not accounted for. It appears that this flow drives the tip secondary vortex inward towards the hub.

The simulation results place the hub secondary flow vortex at 25 percent of span at the exit of the rotor, which is in good agreement with measurements. This vortex, however, appears to be more diffuse than measured, which may account for the lack of a local minimum in the exit flow relative total pressure coefficient at 25 percent of span.

The deviation from the design intent of the rotor relative exit flow angle is shown in Fig. 5. This angle is plotted as a function of span, with the solid curve representing the simulation and the open symbols the measured data from Sharma et al, 1988. The agreement between the two is reasonable with the exception of the tip region, where the result of neglecting the tip leakage flow is quite evident. The noticeable overturning of the flow near the endwalls and the subsequent underturning in the region of midspan caused by the secondary vortices is clearly seen in both the

data and the prediction. The flow physics which leads to this result appears to be well captured.

Recently the authors became aware of data acquired under A.F.O.S.R. sponsorship by United Technologies Research Center which shows the agreement between simulation and measurement to be better than that indicated by Figs. 4 and 5. An evaluation of the present results in light of this data will have to await its publication.

The next two figures are for the second vane. The first, Fig. 6, shows the predicted total pressure coefficient forward and aft of the second vane as a function of span. Also shown is the data from Sharma et al. (1988).
The predicted total pressure coefficients are lower than measured which, as previously noted, is the result of overestimating the loss produced by the first two blade rows. The difference between these two curves is a measure of the loss across the blade row. It too appears to be overestimated. With the exception of the flow region strongly influenced by the tip leakage flow from the rotor, the indicated trends agree with the experiment. Judging by the shape of the incoming total pressure field (either from the data or the prediction) it does not appear that the secondary vortices generated by rotor would have a significant effect on the performance of the second vane. The next figure, which shows the flow angle entering and leaving the second vane relative to the design intent, leads to a far different conclusion. The large variation in the inlet flow angle between 10 and 40 percent of span seen in both the experimental data and prediction clearly is caused by the rotor hub secondary vortex. The time-averaged signature of this vortical structure is a region of shear whose vorticity vector is nearly aligned with the incoming time-averaged velocity field. The tip secondary vortex appears to generate a similar structure; however, the measurements suggests it occurs in board of that predicted. This entering shear flow causes the second vane to behave aerodynamically differently than it would in isolation.

The results shown in Fig. 7 indicate that the simulation predictions are in reasonable agreement with data. The simulation captures the underturning of the flow near the endwalls, and in the midspan region, the tendency for the flow to overturn. This behavior is part due to the time-averaged shear flow produced by the rotor secondary vortices.

The last figure shows the limiting streamline pattern associated with the time-averaged flow adjacent to the second vane pressure surface. Also shown is the corresponding flow visualization result of Langston (Langston, 1988). These results are presented to show that the time-averaged effect of the unsteady vorticity field entering a blade row has a major influence on the flow field within the blade row. Near midspan, the incoming shear flow causes a contraction of the streamlines, suggesting the existence of a line of flow separation. Near both endwalls, the time-averaged vorticity field entering the second vane interacts with the secondary vortices generated within the vane to generate two lines of flow attachment. This flow pattern is far more complicated than that for an isolated blade row and the ability of the present model to capture its structure is very encouraging. Finally, in closing it is suggested that the enhanced heat transfer observed at midspan of the suction surface reported in Sharma et al. (1988) is caused by the secondary vortices generated within the rotor.

SUMMARY AND CONCLUSION

Given the early state of the average passage model development, the results presented in this report are very encouraging. The amount of empirical information used in the stage and one-half turbine simulation is considerably less than that required to achieve comparable results using today's quasi three-dimension flow models. The average passage flow model also appears to be able to capture the physical features of the secondary flow field generated within a multistage turbine configuration. It appears that an accurately modeled of the time-averaged vorticity field produced by the unsteady secondary vorticity exiting a blade row is required to establish the performance of the downstream blade row. The outlined closure procedure, unlike some others which have been suggested, insures that the unsteady vorticity field exiting a blade row is consistent with the exiting time-averaged vorticity field. Hence, no spurious vorticity is produced as a result of coupling one blade row to another.

The simulation of the stage and one-half turbine has shown the complex nature of the endwall flow in a low aspect ratio turbine. In the rotor, the secondary vortices generated within the endwalls affect the flow at midspan. They cause the endwall fluid to deposited on the suction surface. This transport of low momentum fluid leads to significant spanwise mixing across the axisymmetric stream surface. It is doubtful that an endwall boundary layer model could be used to predict this phenomenon.

There are numerous research activities that need to be pursued to further the development of the average passage flow model. Other configurations need to be simulated, including multistage compressors and high- speed machinery. Grid generators need to be developed which are compatible with the average passage model that can cluster grid points in regions of high flow gradients that occur near and away from solid surfaces. Algorithm improvements need to be made to speed convergence. The sensitivity of design parameters to turbulence modeling for the average passage model must be established. Finally, experimental and analytical work in support of closure modeling must be pursued to establish the models for generalized Reynolds stresses and the associated energy correlations.

ACKNOWLEDGEMENTS

The authors wish to express their gratitude to Professor E.M. Greitzer of the Massachusetts Institute of Technology and to Dr. O.P. Sharma of Pratt & Whitney Aircraft for their many useful suggestions during the course of this work. The authors would also like to thank Dr. R.P. Dring of the United Technologies Research Center for providing the experimental pressure distribution data and Dr. L.S. Langston of the University of Connecticut for his flow visualization results.

REFERENCES

Adamczyk, J.J., 1984, "Model Equation for Simulating Flows in Multistage Turbomachinery," ASME Paper 85-GT-226. (NASA TM-86869).

Adamczyk, J.J., Mulac, R.A., and Celestina, M.L., 1986, "A Model for Closing the Inviscid Form of the Average Passage Equation System," ASME Paper 86-GT-227. (NASA TM-87199).

Baldwin, B.S. and Lomax, H., 1978, "Thin Layer Approximation and Algebraic Model for Separated Turbulent Flows," AIAA Paper 78-257.

Brandt, A., 1982, "Guide to Multigrid Development," Multigrid Methods, Springer-Verlag.

Celestina, M.L., Mulac, R.A., and Adamczyk, J.J., 1986, "A Numerical Simulation of the Inviscid Flow Through a Counterrotating Propeller," ASME Paper 86-GT-138.

Dawes, W.N., 1986, "Application of Full Navier-Stokes Solvers to Turbomachinery Flow Problems," Numerical Techniques for Viscous Flow Calculation in Turbomachinery Bladings, VKI-LS-1986-02, Von Karman Institute for Fluid Dynamics, Rhode-Saint-Genese, Belgium.

Denton, J.D. and Singh, U.K., 1979, "Time Marching Methods for Turbomachinery Flow Calculations," Application of Numerical Methods to Flow Calculations in Turbomachines, VKI-LEC-SER-1979-7, Von Karman Institute for Fluid Dynamics, Rhode-Saint-Genese, Belgium.

Dring, R.P., 1988, Private Communication, United Technologies Research Center.

Jameson, A., Rizzi, A., Schmidt, W., and Turkel, E., 1981, "Numerical Solutions of the Euler Equations by Finite Volume Methods Using Runge-Kutta Time-Stepping Schemes," AIAA Paper-81-1259.

Langston, L.S., 1988, Private Communication, University of Connecticut.

Mulac, R.A., 1986, "A Multistage Mesh Generator for Solving the Average Passage Equation System," NASA CR-179539.

Ni, R.H., "Flow Simulation in Multistage Turbine," Presented at the NASA Marshall Space Flight Center Computational Fluid Dynamics Workshop, Apr. 1987.

Rai, M.M., 1987, "Unsteady Three-Dimensional Simulations of Turbine Rotor-Stator Interaction," AIAA Paper 87-2058.

Sharma, O.P., Renaud, E., Butler, T.L., Millsaps, K. Jr., Dring, R.P., and Joslyn, H.G., 1988, "Rotor-Stator Interaction in Multi-Stage Axial-Flow Turbines," AIAA Paper-88-3013.

Smith, L.H., Jr., 1966, "The Radial-Equilibrium Equation of Turbomachinery," Journal of Engineering for Power, Vol. 88, No. 1, pp. 1-12. (Discussion in Vol. 88, No. 3, p. 282).

Vatsa, V.N. and Wedan, B.W., 1988, "Navier-Stokes Solutions for Transonic Flow Over a Wing Mounted in a Tunnel," AIAA Paper-88-0102.

Whitfield, D.L., Swafford, T.W., Janus, J.M., Mulac, R.A., and Belk, D.M., 1987, "Three-Dimensional Unsteady Euler Solutions for Propfans and Counter-rotating Propfans in Transonic Flow," AIAA Paper 87-1197.

Wu, Chung-Hua, 1952, "A General Theory of Three-Dimensional Flow in Subsonic and Supersonic Turbomachines of Axial-, Radial-, and Mixed-Flow Types," NACA TN 2604.

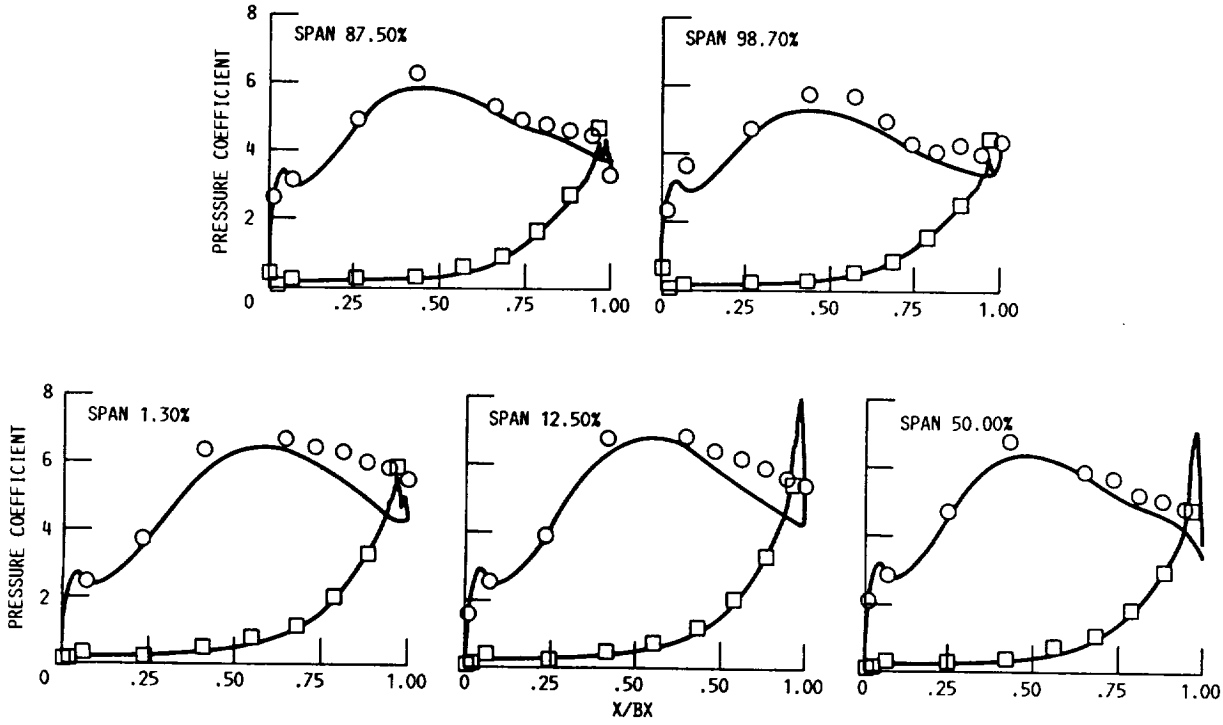

FIGURE 1. - FIRST BLADE PRESSURE DISTRIBUTIONS.

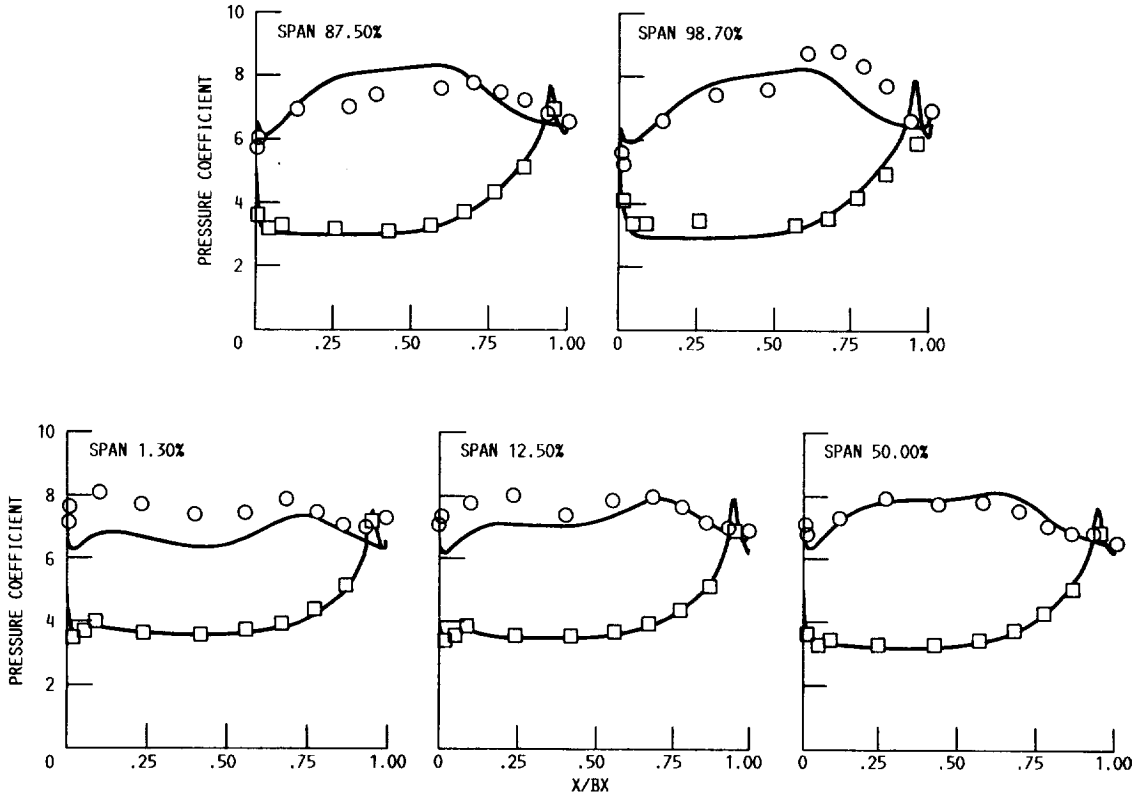

FIGURE 2. - ROTOR PRESSURE DISTRIBUTIONS.

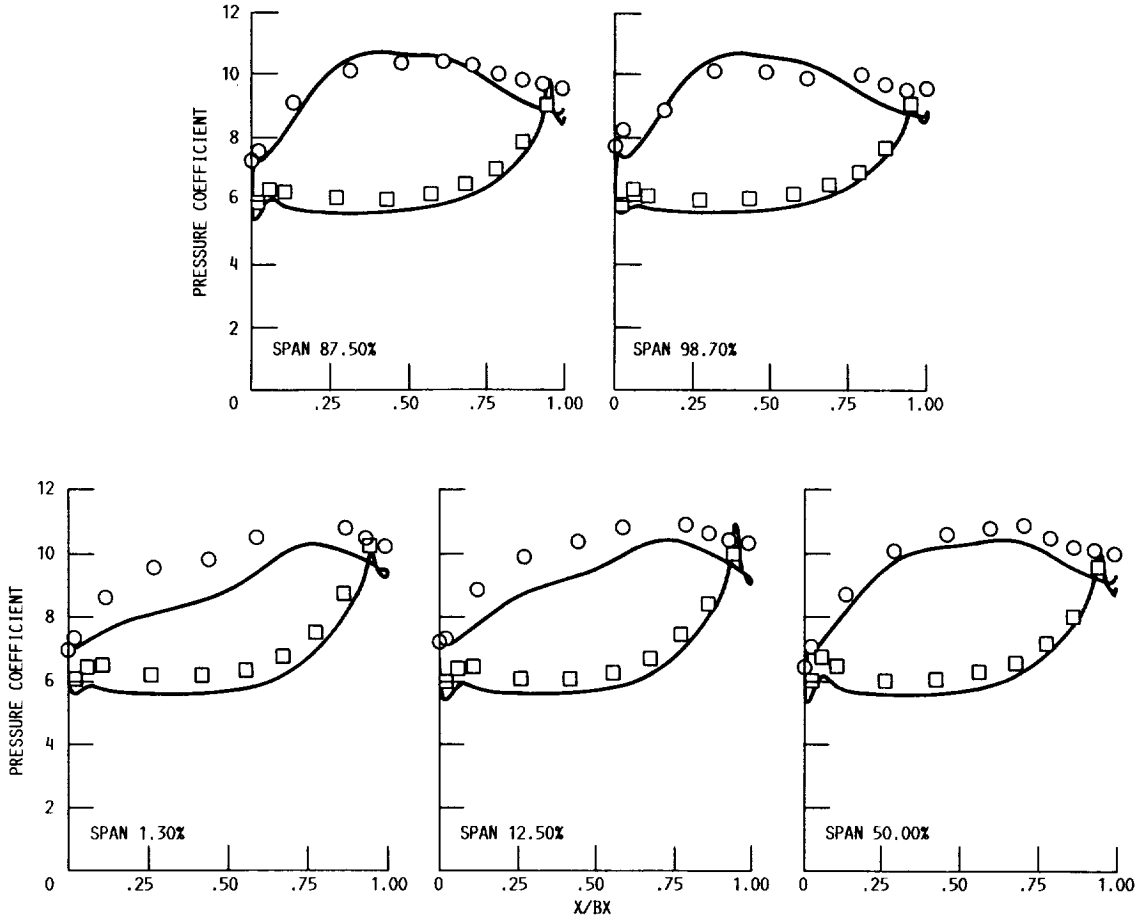

FIGURE 3. - SECOND BLADE PRESSURE DISTRIBUTIONS.

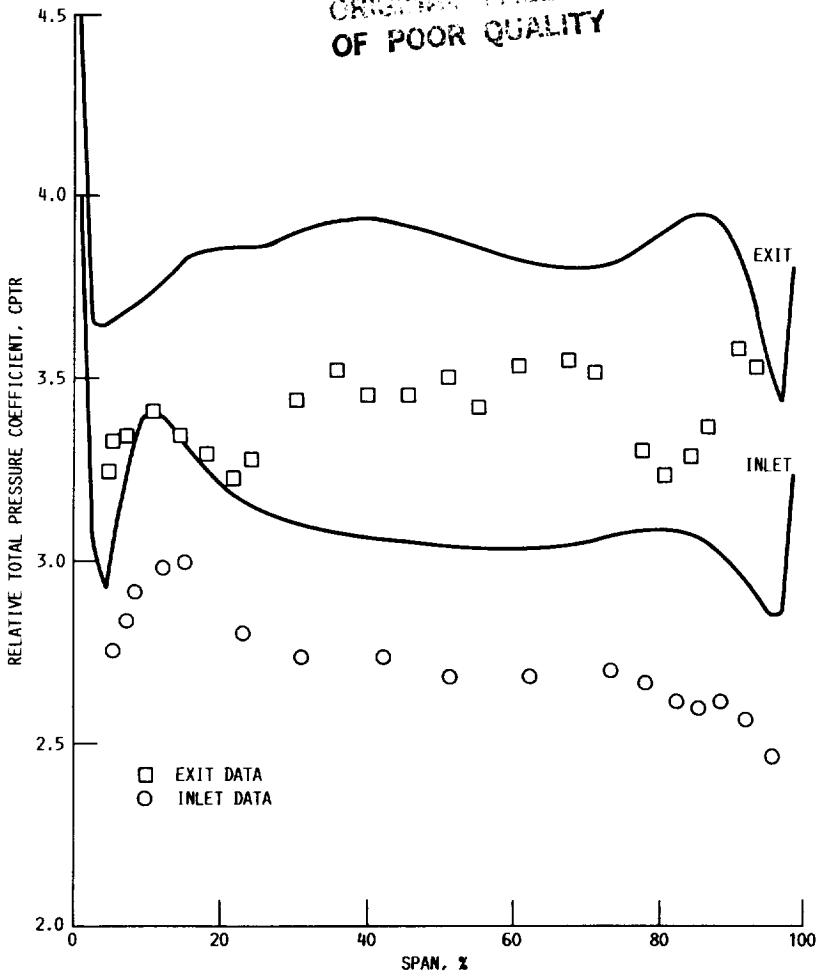

FIGURE 4. - ROTOR RELATIVE TOTAL PRESSURE COEFFICIENT VERSUS SPAN.

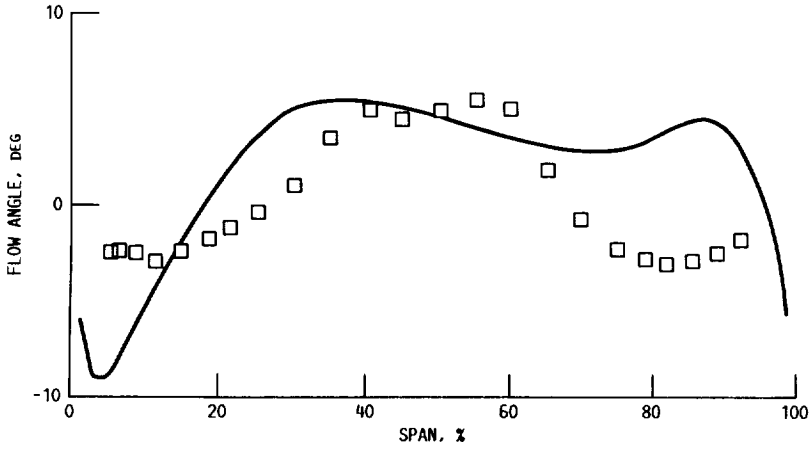

FIGURE 5. - ROTOR RELATIVE EXIT FLOW ANGLE VERSUS SPAN.

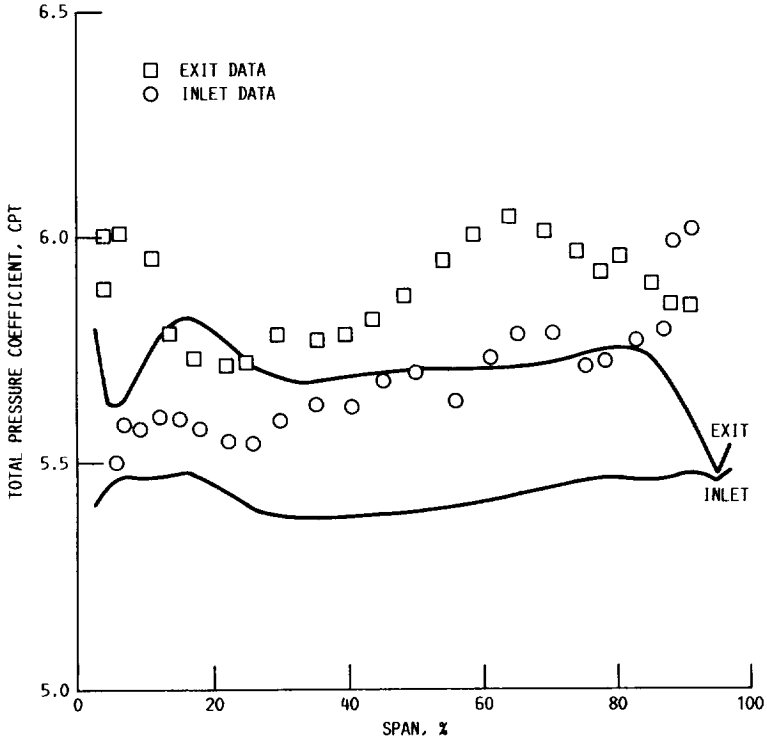

FIGURE 6. - SECOND BLADE TOTAL PRESSURE COEFFICIENT VERSUS SPAN.

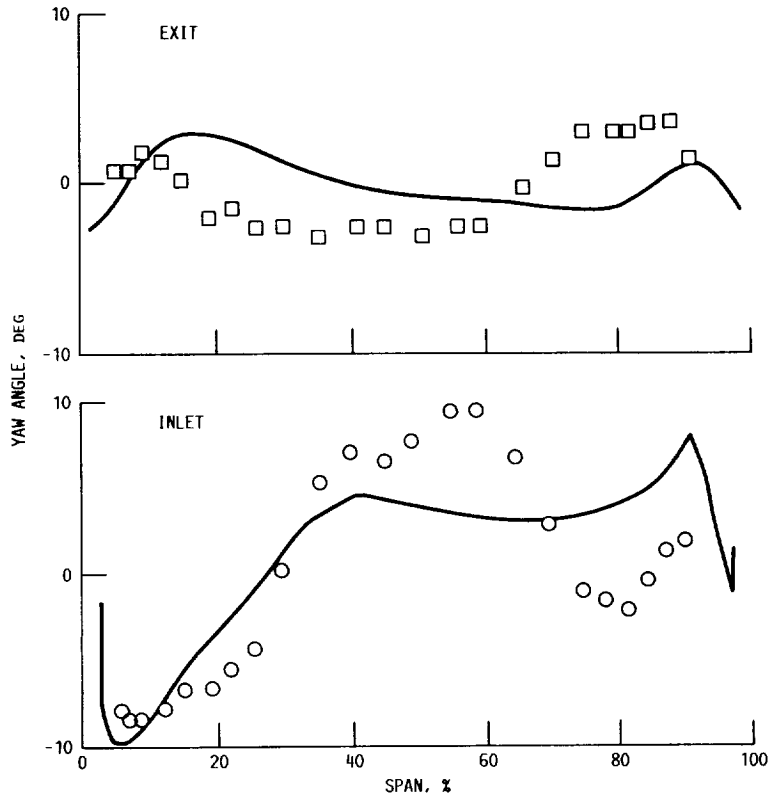

FIGURE 7. - SECOND STATOR FLOW ANGLE DISTRIBUTION.

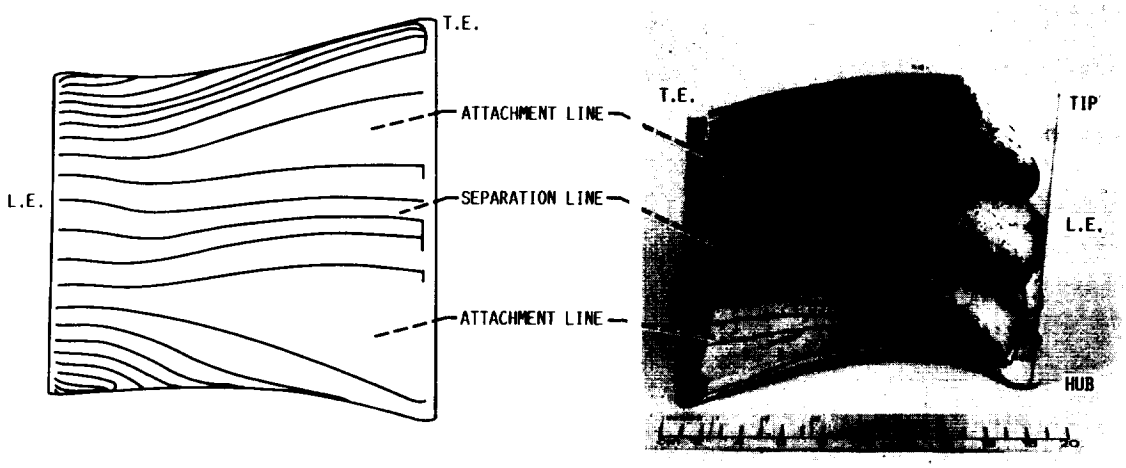

FIGURE 8. - SECOND BLADE PRESSURE SURFACE LIMITING STREAMLINE PATTERN.

NASA
National Aeronautics and Space Administration

Report Documentation Page

1. Report No.	2. Government Accession No.	3. Recipient's Catalog No.
NASA TM-101376		

4. Title and Subtitle	5. Report Date
Simulation of 3-D Viscous Flow Within a Multi-Stage Turbine	6. Performing Organization Code

7. Author(s)	8. Performing Organization Report No.
John J. Adamczyk, Mark L. Celestina, Tim A. Beach and Mark Barnett	E-4430
	10. Work Unit No. 505-90-01

9. Performing Organization Name and Address	11. Contract or Grant No.
National Aeronautics and Space Administration Lewis Research Center Cleveland, Ohio 44135-3191	13. Type of Report and Period Covered Technical Memorandum

12. Sponsoring Agency Name and Address	14. Sponsoring Agency Code
National Aeronautics and Space Administration Washington, D.C. 20546-0001	

15. Supplementary Notes

Prepared for the 34th International Gas Turbine and Aeroengine Congress and Exposition sponsored by the American Society of Mechanical Engineers, Toronto, Canada, June 4-8, 1989.

16. Abstract

This work outlines a procedure for simulating the flow field within multistage turbomachinery which includes the effects of unsteadiness, compressibility, and viscosity. The associated modeling equations are the average passage equation system which governs the time-averaged flow field within a typical passage of a blade row embedded within a multistage configuration. The results from a simulation of a low aspect ratio stage and one-half turbine will be presented and compared with experimental measurements. It will be shown that the secondary flow field generated by the rotor causes the aerodynamic performance of the downstream vane to be significantly different from that of an isolated blade row.

17. Key Words (Suggested by Author(s))	18. Distribution Statement
Multistage turbomachinery	Unclassified – Unlimited Subject Category

19. Security Classif. (of this report)	20. Security Classif. (of this page)	21. No of pages	22. Price*
Unclassified	Unclassified	12	A03

NASA FORM 1626 OCT 86

*For sale by the National Technical Information Service, Springfield, Virginia 22161